Numerical ensemble study of ergodic properties of the quartic Fermi-Pasta-Ulam chain. II. Distribution and correlation functions

B. I. Henry
Department of Theoretical Physics, Research School of Physical Sciences, The Australian National University, Canberra, Australian Capital Territory 2601, Australia

J. Grindlay
Guelph-Waterloo Program for Graduate Work in Physics, Waterloo Campus, Waterloo, Ontario, Canada N2L 3G1
(Received 18 January 1989)

Statistical equilibrium data from a time-ensemble data bank, generated for an anharmonic (15+2)-particle chain [Henry and Grindlay, Phys. Rev. A **38**, 2594 (1988)], have been used to calculate coarse-grained distributions for odd-mode velocities, particle velocities, and nearest-neighbor spring extensions. Each distribution proves to be Maxwellian in form. The mode-velocity temperatures agree with the mode-energy temperatures reported previously (Henry and Grindlay, *ibid.*). The time-ensemble data were also used to calculate averages and correlation functions for odd-mode energies, odd-mode velocities, particle velocities, spring energies, and their products. The dynamical response of the chain in the statistical equilibrium regime is found to be largely described by the behavior of modes 11, 13, and 15. These modes prove to be strongly correlated. The corresponding averages and correlation functions are calculated for a microcanonical ensemble of eight harmonic oscillators and compared with the time-ensemble results for the chain.

I. INTRODUCTION

In three earlier papers [1-3] we applied the idea of ensembles[4] to the analysis of the dynamical behavior of a (15+2)-particle chain. The two end particles are held fixed and each particle interacts with its nearest neighbors via linear plus cubic conservative forces. Previous authors[5] had suggested that, when this chain is excited in the 11th mode, it relaxes to equilibrium in some 200 model time units (or "seconds"). The presence of large mode energy fluctuations in the putative equilibrium state made this suggestion at best plausible. To investigate further the question of equilibrium in this chain we generated a numerical, constant-energy statistical ensemble. We integrated the 15 equations of motion numerically for 101 different starting conditions but a common total energy (see Sec. II below), and stored the particle position and velocity data at 1 "second" intervals over a period of 300 "seconds." From this data bank we calculated a coarse-grained energy distribution for each mode as a function of time (because of the effects of round-off error, we restricted the time interval to 250 s). For *each* mode, the corresponding Boltzmann H function[4,6] dropped off to a minimum value at about 200 s, and maintained this value, with minor fluctuations, to the end of the 250-s interval. This type of behavior is generally accepted as indicating an approach to statistical equilibrium.[4,6] The much smaller fluctuations of the mode H functions, compared with the mode energies, provided us with the evidence of relaxation we were looking for. This was further confirmed by the fact that in the statistical equilibrium regime (200 s, 250 s) the odd-mode-energy coarse-grained distributions exhibited[2] Maxwell-Boltzmann forms, in agreement with an algebraic analysis of the three conditions: (i) the H function is a minimum for each mode, (ii) the number of ensemble copies for each mode is a constant, in our case 101, and (iii) the total energy of the chain is a constant. The mode temperatures determined from these distributions ranged over two orders of magnitude. The solutions to the equations of motion of the particles are reversible, since the interparticle forces are conservative. Thus from our statistical-ensemble analysis, we have evidence for a reversible approach to a statistical equilibrium state, characterized by mode-energy Maxwell-Boltzmann distributions and no thermal equilibrium—an interesting collection of thermodynamic and nonthermodynamic properties in a 17-particle chain.

By using higher-precision FORTRAN, we extended the integration of one of these histories to 600 s before round-off error became significant.[3] The particle positions and velocities were stored at 0.1-s intervals over this period. From the statistical-ensemble evidence, we assumed that the (200 s, 600 s) data described a statistical equilibrium regime. Treating these data as a time ensemble,[7] we calculated equilibrium mode-energy coarse-grained distributions. These also proved to have Maxwell-Boltzmann forms with a set of mode-temperature values in agreement with the set obtained from the statistical ensemble. Thus a time sampling and a history sampling yield the same mode-energy distributions, i.e., the constant-energy surface in the 16-dimensional Γ space for the odd modes is ergodic[8] in the segment accessed by these histories. The histories are also very sensitive to initial conditions,[3] i.e., are chaotic,[9] a fact that we believe is not unrelated to the ergodicity.

The work described above dealt with the probability

distribution functions for single modes; that is, the probability of, for example, the jth mode (in equilibrium) having energy in the range $[\varepsilon_j, \varepsilon_j + d\varepsilon_j]$. Two other questions come to mind. First of all, do other properties of the chain (mode velocity, particle velocity, etc.) exhibit exponential distributions in the statistical equilibrium regime? The fact that the mode velocities and particle velocities approximately satisfy the equipartition theorem[2,4] suggests that these two quantities do. Second, there is the more general question of, what is the form of the probability distribution function or density of states in the Γ space of the chain? We can make two comments about this latter function: (i) from the mode-energy results described above, the probability distribution is clearly not a constant, as is the case for the constant energy or microcanonical ensemble of statistical mechanics;[4,6] and (ii) the large fluctuations in the mode energies are evidence of strong interactions between the modes, and hence we cannot expect the system probability density to be a simple product of single probability densities; in other words, we should expect significant correlations between the dynamical properties of different modes. In this paper we show that the mode velocities, the particle velocities, and the spring extensions each exhibit Maxwellian distributions in the statistical equilibrium regime; we also show that, indeed, the off-diagonal correlations for these quantities are significant. Because of the ergodic nature of this region of Γ space, we are free to use either the statistical or the time ensemble for this type of analysis. We have chosen the latter option.

The material in the remainder of this paper is presented as follows. In Sec. II we give a brief description of the (15+2)-particle chain model and the numerical analysis leading to the time-ensemble data bank. Section III contains a discussion of the correlation functions for the mode energies and a comparison of these results with the case of an isolated system with eight harmonic oscillators. In Secs. IV–VI we describe the distributions and correlations of the mode velocities, the particle velocities, and the spring extensions, respectively. The last section, Sec. VII, contains a brief discussion of our results.

II. MODEL

Consider a (15+2)-particle chain with particle labels $n=0,1,\ldots 15,16$. We assume clamped ends and nearest-neighbor linear and cubic forces. The displacement of the nth particle is denoted by x_n; the boundary conditions and equations of motion are written as

$$x_0 \equiv x_{16} \equiv 0 \ , \tag{1}$$

$$\ddot{x}_n = (x_{n+1} - 2x_n + x_{n-1}) + \mu[(x_{n+1}-x_n)^3 - (x_n - x_{n-1})^3] \ , \tag{2}$$

for $n=1,2,\ldots,14,15$; μ represents the nonlinear force constant in these dimensionless units. The normal-mode coordinates q_j are defined as

$$q_j = (1/2\sqrt{2}) \sum_{n=1}^{15} x_n \sin(jn\pi/16) \ , \tag{3}$$

and corresponding frequencies

$$\omega_j = 2\sin(j\pi/32) \ . \tag{4}$$

We introduce mode energies

$$\varepsilon_j = (\dot{q}_j^2 + \omega_j^2 q_j^2)/2 + (\mu/4) \sum_{k,l,m=1}^{15} A_{j,k,l,m} q_j q_k q_l q_m \ . \tag{5}$$

The coefficients $A_{j,k,l,m}$ are defined in Refs. 2 and 3.

The time-ensemble data bank was constructed as follows.[3] Using quadruple-precision FORTRAN, we carried out a numerical integration of the equations of motion (2) for the case $\mu=0.8$, total energy $E_0=10$, and initial condition—the 11th mode displaced and released from rest. The integration algorithm was a predictor-corrector multistep method[10,11] with a time step of 0.01. The dynamic history between 200 and 600 s is free of round-off error to better than 0.02%, and describes a set of statistical equilibrium states of the system.[3] The chain particle positions and velocities at 0.1-s intervals in the range (200 s, 600 s) made up our equilibrium time ensemble.

III. MODE ENERGIES

The time dependence of the mode Boltzmann H functions and the numbers in both the statistical- and time-ensemble data banks show that in statistical equilibrium the mode-energy distributions possess a Maxwell-Boltzmann form.[2,3] The large flows of energy between the modes indicate that the time dependence of the energies in different modes is likely to be strongly correlated. We note that the constraint of constant total system energy imposes correlations even in the absence of mode-mode coupling (see Appendix A and additional comments below).

Define the correlation function for mode energies $\varepsilon_j(t)$ and $\varepsilon_k(t)$ as

$$C(\varepsilon_j, \varepsilon_k) \equiv \overline{\varepsilon_j \varepsilon_k} - \bar{\varepsilon}_j \bar{\varepsilon}_k \ , \tag{6}$$

where the bar indicates a time average. We calculated the correlation functions for the energies of the eight odd modes (the even modes are forbidden with the initial condition imposed here[2]) using data from the time ensemble in the equilibrium period (200 s, 600 s). The results are shown in Fig. 1. The largest correlation element is $C(\varepsilon_{15},\varepsilon_{15}) = 0.0421 E_0^2$; E_0 is the total energy of the system. The $C(\varepsilon_j,\varepsilon_k)$ elements are all normalized to this value in Fig. 1. The diagonal elements decrease monotonically with decreasing mode index to the value $C(\varepsilon_1,\varepsilon_1) = 0.748\times 10^{-5} E_0^2$. The off-diagonal elements display both positive and negative values, and tend to drop in magnitude away from the $C(\varepsilon_{15},\varepsilon_{15})$ position—they range in value from

$$C(\varepsilon_{13},\varepsilon_{15}) = -0.0276 E_0^2 \ \text{ to } \ C(\varepsilon_5,\varepsilon_{15}) = 0.000\,561 E_0^2 \ . \tag{7}$$

It is clear that there are strong correlations between mode energies and that modes 11, 13, and 15 dominate the dynamic response of the system in the statistical equi-

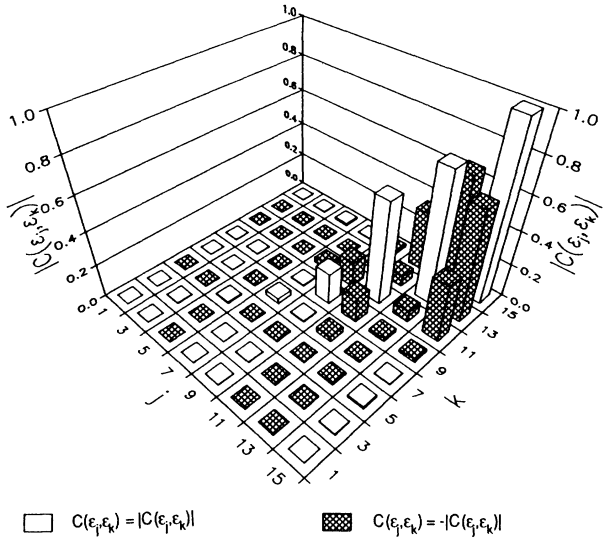

FIG. 1. Three-dimensional histogram of the correlation function $C(\varepsilon_j,\varepsilon_k)$ for the energies ε_j of the eight odd modes. The cross hatching indicates negative values. The columns have been normalized to the maximum value $C(\varepsilon_{15},\varepsilon_{15})=0.0421E_0^2$.

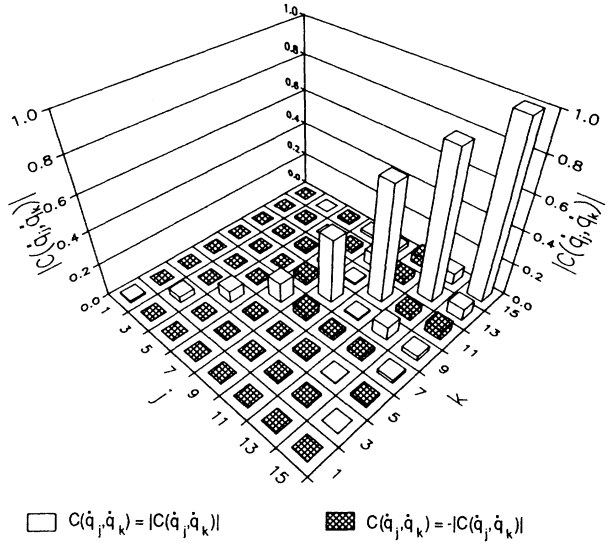

FIG. 2. Three-dimensional histogram of the correlation function $C(\dot{q}_j,\dot{q}_k)$ of the velocities q_j of the eight odd modes. The cross hatching indicates negative values. The columns have been normalized to the maximum value $C(\dot{q}_{15},\dot{q}_{15})=0.0352E_0$.

librium regime.

It is interesting to compare this behavior with that of the microcanonical ensemble of eight harmonic oscillators. This latter system is free of any mode coupling but is subjected to the constraint of constant total energy. We discuss this case in Appendix A and find that

$$C(\varepsilon_j,\varepsilon_j)=0.0122E_0^2,\quad C(\varepsilon_j,\varepsilon_k)=-0.001\,74E_0^2,\quad j\neq k\ . \tag{8}$$

This pattern of behavior is quite different from the interacting-modes case—the diagonal elements are equal and the off-diagonal elements are both equal and negative.

IV. MODE VELOCITIES

The average mode velocity $\bar{\dot{q}}_j$ and the average mode velocity squared $\overline{\dot{q}_j^2}$ calculated from the time-ensemble data in the statistical equilibrium regime are shown in Table I. The correlation functions $C(\dot{q}_j,\dot{q}_k)$ and $C(\dot{q}_j^2,\dot{q}_k^2)$ determined from the same data are shown in Figs. 2 and 3, respectively. As before, these figures are normalized to the largest value, namely, $C(\dot{q}_{15},\dot{q}_{15})=0.352E_0$ and $C(\dot{q}_{15}^2,\dot{q}_{15}^2)=0.131E_0^2$. The diagonal elements decrease monotonically with decreasing mode index to the values $0.004\,26E_0$ and $0.000\,018\,6E_0^2$, respectively. In the case of $C(\dot{q}_j,\dot{q}_k)$ the off-diagonal elements range from

$$C(\dot{q}_{11},\dot{q}_{15})=-0.0214E_0\ \text{ to }\ C(\dot{q}_9,\dot{q}_{13})=0.0286E_0\ . \tag{9}$$

In a bounded system with conservative forces, such as the (15+2)-particle chain, one might expect that, over the long term, the average mode velocities $\bar{\dot{q}}_j$ and the off-diagonal mode-correlation elements $C(\dot{q}_j,\dot{q}_k)$, $j\neq k$, should be zero. Thus we interpret the nonvanishing $\bar{\dot{q}}_j$, in Table I, and the nonvanishing off-diagonal elements, in Fig. 2, as errors arising from the smallness of our 4001-element data bank. The largest off-diagonal element $C(\dot{q}_{15},\dot{q}_{13})$ is 7% of $C(\dot{q}_{15},\dot{q}_{15})$. The corresponding harmonic results (Appendix A) are

$$\bar{\dot{q}}_j=0,\quad C(\dot{q}_j,\dot{q}_j)=0.125E_0,\quad C(\dot{q}_j,\dot{q}_k)=0,\quad j\neq k\ . \tag{10}$$

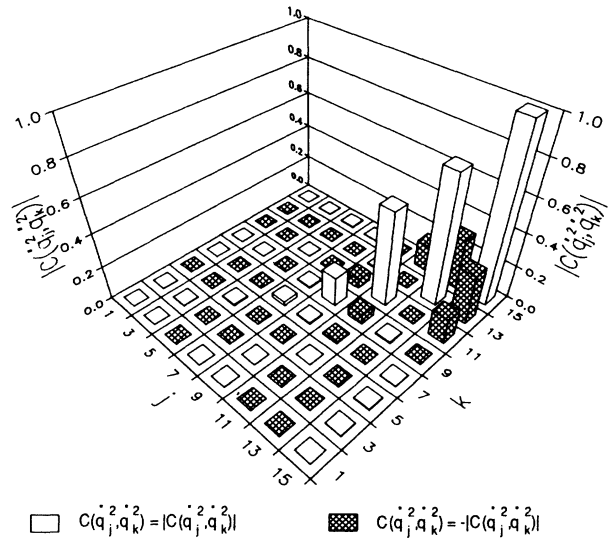

FIG. 3. Three-dimensional histogram of the correlation function $C(\dot{q}_j^2,\dot{q}_k^2)$ for the square of the velocities of the eight odd modes. The cross hatching indicates negative values. The columns have been normalized to the maximum value $C(\dot{q}_{15}^2,\dot{q}_{15}^2)=0.131E_0^2$.

TABLE I. Average odd-mode velocities and odd-mode velocities squared, calculated from the equilibrium time-ensemble data. Distribution temperatures are $\overline{\Theta}_j$ for the odd-mode energies, and $\Theta_j^{\dot{q}}$ for odd-mode velocities determined from the time ensemble (Ref. 3) and $\langle \overline{\Theta}_j \rangle$ for the odd-mode energies determined from the statistical ensemble (Ref. 2).

j	$\bar{q}_j$	$\dot{q}_j^{\Sigma}$	$\overline{\Theta}_j$	$\langle \overline{\Theta}_j \rangle$	$\Theta_j^{\dot{q}}$
1	−0.0026	0.04	0.04	0.01	0.04
3	0.0005	0.13	0.15	0.08	0.15
5	0.0024	0.25	0.22	0.21	0.24
7	0.0008	0.43	0.36	0.36	0.38
9	−0.0031	1.38	1.00	1.26	1.07
11	−0.0033	2.45	2.83	2.21	2.59
13	−0.0038	3.05	3.03	3.22	3.04
15	0.0012	3.52	4.90	3.54	3.73

The correlation function for the square of the mode velocities, Fig. 3, shows a similar pattern to that for the mode energies, Fig. 1. The modes 11, 13, and 15 dominate. The off-diagonal elements lie in the range

$$C(\dot{q}_{13}^2,\dot{q}_{15}^2)=-0.0392E_0^2 \text{ to } C(\dot{q}_9^2,\dot{q}_{13}^2)=0.001\,15E_0^2 . \tag{11}$$

This indicates strong correlations between the modes and contrasts with the harmonic behavior, Appendix A, where

$$C(\dot{q}_j^2,\dot{q}_j^2)=0.0260E_0^2, \quad C(\dot{q}_j^2,\dot{q}_k^2)=-0.001\,74E_0^2 \tag{12}$$

with $j\neq k$.

The average mode velocity squared is approximately

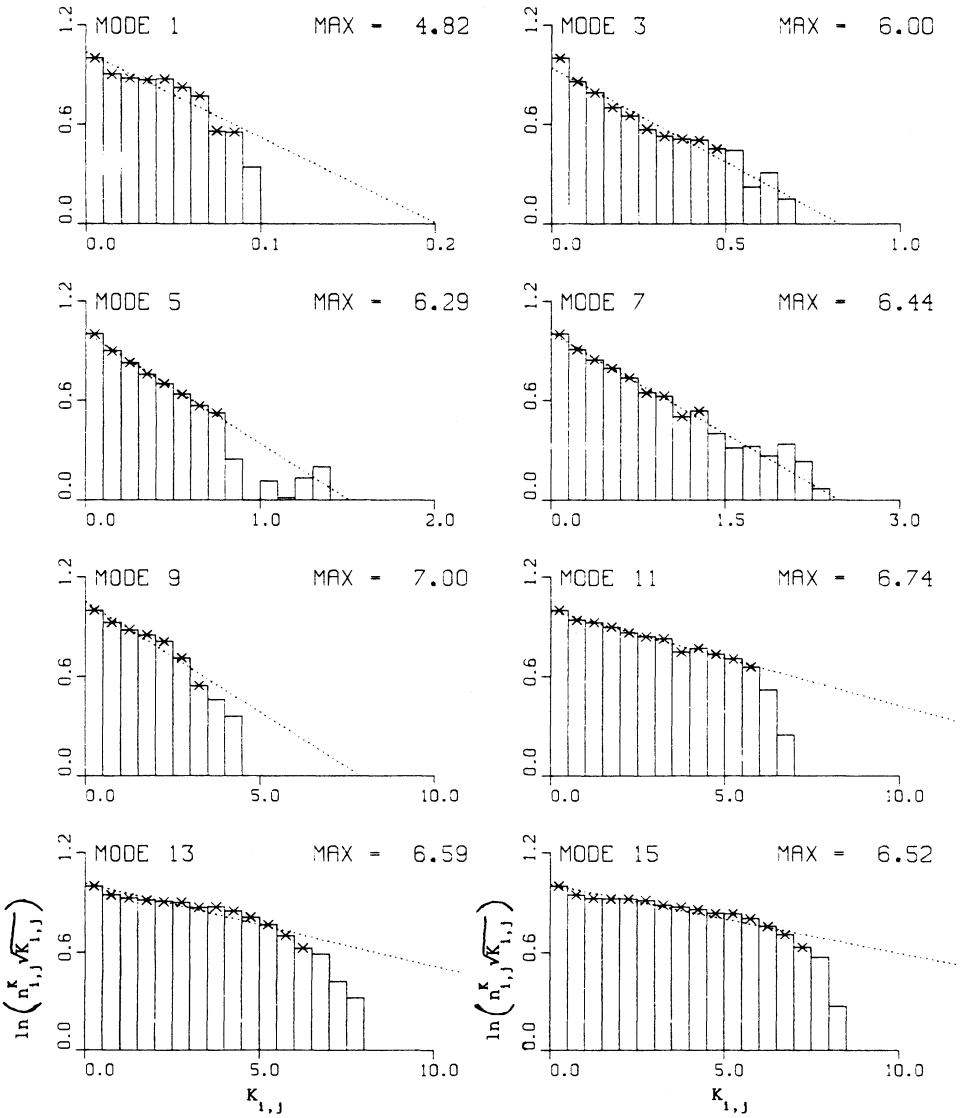

FIG. 4. Histograms of $\ln(n_{i,j}^K\sqrt{K_{i,j}})$ vs the partition kinetic energy $K_{i,j}$, for the eight odd modes. $n_{i,j}^K$ is the coarse-grained kinetic energy distribution for the jth mode. The columns are normalized to the value shown in the top right corner of each graph. The crosses indicate points with $n_{i,j}\geq 20$. The dashed line is a best-fit straight line through the crosses.

equal to the corresponding mode temperature (see Table I columns headed $\overline{\dot{q}_j^2}$, $\overline{\Theta}_j$, and $\langle\overline{\Theta}_j\rangle$); this suggests that the mode-velocity distribution is Maxwellian, Appendix B. Assuming this conclusion to be true, we write the number of j-mode copies with mode velocity in the range $[\dot{q}_j, \dot{q}_j+d\dot{q}_j]$ in the form

$$dn_j^{\dot{q}}=c_j\exp-(K_j/\Theta_j^{\dot{q}})d\dot{q}_j \ , \tag{13}$$

where $K_j\equiv\dot{q}_j^2/2$ is the kinetic energy and $\Theta_j^{\dot{q}}$ the velocity distribution temperature of the jth mode. From this result, the number of j-mode copies with kinetic energy in the range $[K_j, K_j+dK_j]$ is

$$dn_j^K=\{2c_j\exp[-(K_j/\Theta_j^{\dot{q}})]/\sqrt{K_j}\}dK_j \ . \tag{14}$$

To check the validity of this form for the distribution function (13), we followed the approach used for the mode-energy distributions.[2,3] For the jth mode, the kinetic interval $(0,E_0)$ was divided into N_j elementary cells with individual extensions E_0/N_j. At each of the 4001-data points in the equilibrium regime of the time ensemble, the jth mode has a certain kinetic energy. The coarse-grained kinetic energy distribution is described by $n_{i,j}^K$, the number of j-mode samples with kinetic energy in the range $[(i-1)E_0/N_j, iE_0/N_j]$, $i=1,2,\ldots,N_j$. To the ith partition we describe the kinetic energy

$$K_{i,j}=(i-\tfrac{1}{2})E_0/N_j \ . \tag{15}$$

If the kinetic energy distribution is given by (14). then the coarse-grained distribution is

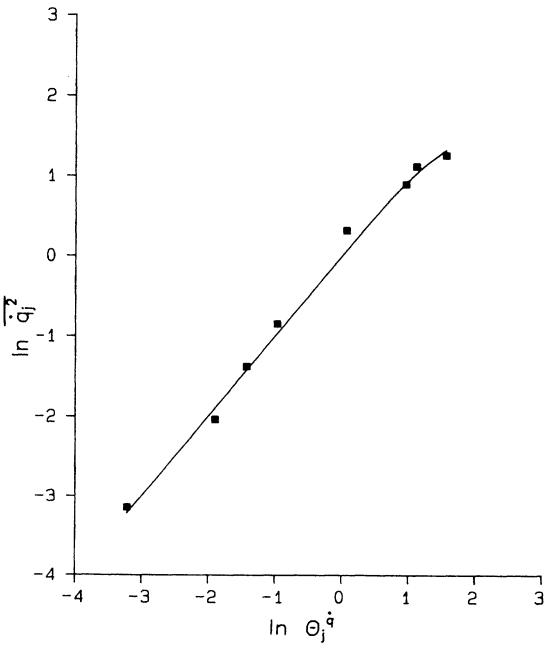

FIG. 5. Log-log scale graph of the average mode velocity squared vs mode-velocity temperature, Eqs. (B4) and (B5), with system energy $E_0=10$. The squares indicate the points $(\Theta_j^{\dot{q}},\overline{\dot{q}_j^2})$, $\Theta_k^{\dot{q}}$ is the mode-velocity temperature, Table I, and $\overline{\dot{q}_j^2}$ the time average of the square of the mode velocity, Table I.

$$n_{i,j}^K=A_j\exp-(K_{i,j}/\Theta_j^{\dot{q}})/\sqrt{K_{i,j}} \ . \tag{16}$$

A_j is a normalization constant. It follows from (15) and (16) that $\ln(n_{i,j}^K\sqrt{K_{i,j}})$ is a linear function of the cell index i. Histograms of $\ln(n_{i,j}^K\sqrt{K_{i,j}})$ versus $K_{i,j}$ calculated from the time-ensemble equilibrium data, are shown in Fig. 4 for each of the odd modes; the N_j values chosen are $N_1=1000$, $N_3=200$, $N_5=67$, and $N_j=20$, $j=9$, 11, 13, and 15. As before,[2] we neglect statistically small values (less than 20) of $n_{i,j}$ and find the least-squares straight-line best fit (the dashed line) through the remaining points (marked with a cross). From the slopes of these lines we calculated the associated mode-velocity distribution temperatures $\Theta_j^{\dot{q}}$; see Table I. For comparison we have also listed the mode-energy distribution temperatures determined from the statistical[2] and the time[3] ensembles. From Fig. 4 and Table I we conclude that (a) the mode velocities in the equilibrium regime are distributed in a Maxwellian form (13), and (b) the mode-velocity temperature is equal to the mode-energy temperature for each mode.

As an additional check on the exponential form, we note that $\overline{\dot{q}_j^2}$ is an implicit function of the temperature Θ and the system energy E_0, Eqs. (B4) and (B5). In Fig. 5 we have drawn, on a log-log scale, this function $\overline{\dot{q}^2}$ versus Θ for $E_0=10$; we have also added the points $(\Theta_j^{\dot{q}},\overline{\dot{q}_j^2})$, where Θ_j are the mode-temperature values determined from the slopes in Fig. 4, and $\overline{\dot{q}_j^2}$ are the averages determined from the time ensemble (see Table I for both quantities). The satisfactory fit also confirms the Maxwellian form.

V. PARTICLE VELOCITIES

The average particle velocities $\overline{\dot{x}_n}$ and the average squares of particle velocities $\overline{\dot{x}_n^2}$, determined from the equilibrium regime of the time ensemble, are listed in Table II. We recall that in the absence of the even modes the displacements satisfy the identity $x_n\equiv x_{16-n}$ for $n=1,2\ldots7$, and hence we need only list the eight independent quantities $\overline{\dot{x}_n^2}$, $n=1,2,\ldots,8$. The pattern of $\overline{\dot{x}_n^2}$ values in Table II is consistent with the local environment similarities and differences of the particles—similar interactions for particles 2,3,...,7, different "interaction" for the end particle 1, and different effective mass for

TABLE II. Time-averaged particle velocities and particle velocities squared, $n=1,2,..,8$. Distribution temperature $\Theta_n^{\dot{x}}$ for the particle velocities from equilibrium time-ensemble data.

n	$\overline{\dot{x}_n}$	$\overline{\dot{x}_n^2}$	$\Theta_n^{\dot{x}}$
1	−0.0018	0.52	0.49
2	0.0033	0.78	0.82
3	−0.0008	0.61	0.62
4	−0.0023	0.77	0.82
5	−0.0008	0.79	0.74
6	−0.0013	0.68	0.64
7	0.0004	0.73	0.64
8	−0.0022	1.48	1.47

$n=8$ (this is the only particle not forced to vibrate in unison with another—the odd-mode condition mentioned above).

The correlation functions, also calculated from the time ensemble, $C(\dot{x}_n,\dot{x}_m)$ and $C(\dot{x}_n^2,\dot{x}_m^2)$, are shown in Figs. 6 and 7. The normalization values used in these figures are $C(\dot{x}_8,\dot{x}_8)=0.148E_0$ and $C(\dot{x}_8^2,\dot{x}_8^2)=0.0351E_0^2$, respectively. The minimum diagonal components and the range of off-diagonal components are for $C(\dot{x}_n,\dot{x}_m)$, $C(\dot{x}_1,\dot{x}_1)=0.0518E_0$, and

$$C(\dot{x}_7,\dot{x}_8)=-0.0861E_0 \text{ to } C(\dot{x}_4,\dot{x}_6)=0.0186E_0 , \quad (17)$$

and for $C(\dot{x}_n^2,\dot{x}_m^2)$, $C(\dot{x}_1^2,\dot{x}_1^2)=0.004\,37E_0^2$ and

$$C(\dot{x}_6^2,\dot{x}_8^2)=-0.0035E_0^2 \text{ to } C(\dot{x}_7^2,\dot{x}_8^2)=0.00721E_0^2 . \quad (18)$$

This contrasts with the harmonic results in Eqs. (10) and (12).

The mode coordinates q_j and the particle coordinates x_n are related by the normal-mode transformation (3). Hence

$$\dot{\bar{x}}_n=(1/2\sqrt{2})\sum_{j=1}^{15}\dot{\bar{q}}_j\sin(jn\pi/16) , \quad (19)$$

$$\overline{\dot{x}_n\dot{x}_m}=\tfrac{1}{8}\sum_{j=1}^{15}\sum_{k=1}^{15}\overline{\dot{q}_j\dot{q}_k}\sin(jn\pi/16)\sin(km\pi/16) . \quad (20)$$

Our speculation in Sec. IV that $\dot{\bar{q}}_j=0$ and $C(\dot{q}_j,\dot{q}_k)=0$, $j\neq k$, implies that (a) $\dot{\bar{x}}_n=0$, in agreement with the very small values displayed under the $\dot{\bar{x}}_n$ column, and (b)

$$\overline{\dot{x}_n\dot{x}_m}=\tfrac{1}{8}\sum_{j=1}^{15}\overline{\dot{q}_j^2}\sin(jn\pi/16)\sin(jm\pi/16) . \quad (21)$$

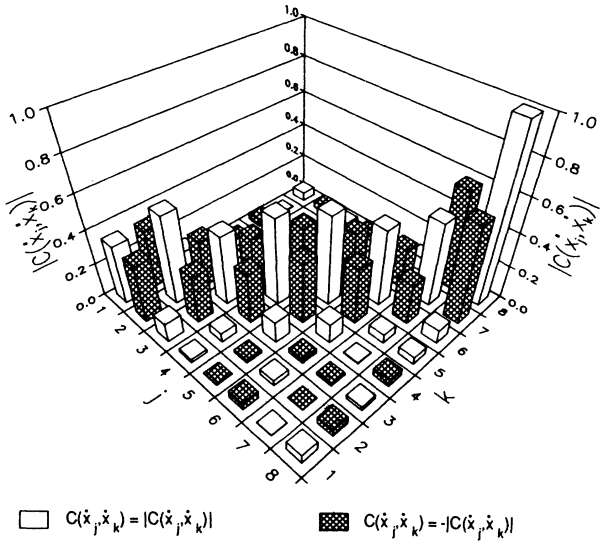

FIG. 6. Three-dimensional histogram of the correlation function $C(\dot{x}_n,\dot{x}_m)$ of the velocities $\dot{x}_n$ of the first eight particles. The cross hatching indicates negative values. The columns have been normalized to the maximum value $C(\dot{x}_8,\dot{x}_8)=0.0148E_0$.

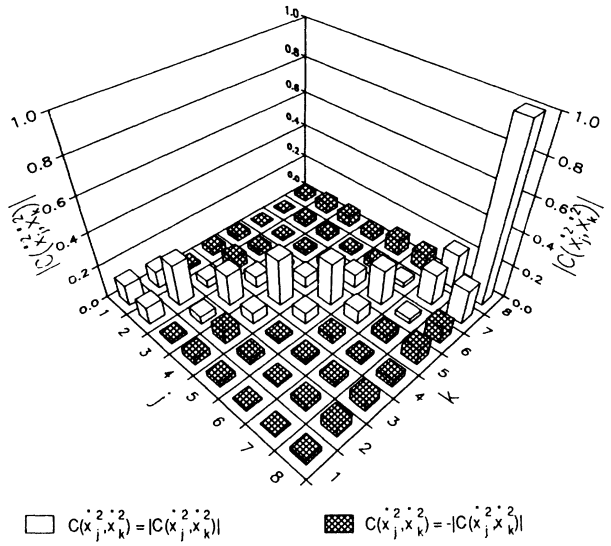

FIG. 7. Three-dimensional histograms of the correlation function $C(\dot{x}_n^2,\dot{x}_m^2)$ of the square of the velocities of the first eight particles. The cross hatching indicates negative values. The columns have been normalized to the maximum value $C(\dot{x}_8^2,\dot{x}_8^2)=0.0351E_0^2$.

When the $\dot{q}_j^2$ values from Table II are substituted in (21) and the sum carried out, we obtain agreement with the diagonal and immediately off-diagonal elements of $C(\dot{x}_n,\dot{x}_m)$ in Fig. 6 to better than 80%. The remaining elements are small, Fig. 6. This suggests that $C(\dot{x}_n,\dot{x}_m)$ is a tridiagonal array simply related to a diagonal array $C(\dot{q}_j,\dot{q}_k)$ through the mode transformation (3). When we substitute the harmonic result $\overline{\dot{q}_j^2}$ independent of j, Eq. (A24), in (21). We find that $\overline{\dot{x}_n^2}$ is a constant independent of n and that the off-diagonal elements $\overline{\dot{x}_n\dot{x}_m}$ vanish. Thus the strong nearest-neighbor negative correlations seen in Fig. 6 are a direct result of anharmonic nearest-neighbor forces in the chain.

The analysis to date[1-3] gives us no clue as to the form of the particle-velocity distribution in either the statistical or the time ensemble. We assume a Maxwellian distribution and check its validity using the time ensemble. For a Maxwellian distribution the number of copies with particle velocity in the range $[\dot{x}_n, \dot{x}_n+d\dot{x}_n]$ is

$$dn_n^{\dot{x}}=c_n\exp-(T_n/\Theta_n^{\dot{x}})d\dot{x}_n , \quad (22)$$

where c_n is a normalization constant, $T_n\equiv\dot{x}_n^2/2$ is the kinetic energy, and $\Theta_n^{\dot{x}}$ the velocity-distribution temperature of the nth particle. From this expression we calculate the number of ensemble copies with particle kinetic energy T_n in the range $[T_n, T_n+dT_n]$, namely,

$$dn_n^T=[2c_n\exp-(T_n/\Theta_n^{\dot{x}})/\sqrt{T_n}]dT_n . \quad (23)$$

Replacing the mode index j with the particle index n, we follow the procedure described in Sec. IV for checking the mode-velocity distribution. We generate a coarse-grained particle kinetic energy distribution with N_n ele-

mentary cells in the interval $(0,E_0)$, where $N_n=50$ for $n=1,2,2,\ldots,7$ and $N_8=27$. We ascribe a kinetic energy $T_{i,n}$, (11), to the ith cell and nth particle. If the kinetic energy distribution is given by (22), then the corresponding coarse-grained particle kinetic energy distribution is

$$n_{i,n}^{T}=A_n\exp[-(T_{i,n}/\Theta_m^{\dot{x}})]/\sqrt{T}_{i,n}\ . \tag{24}$$

Again $\ln(n_{i,n}^{T}\sqrt{T}_{i,n})$ versus i is a straight line with slope proportional to $1/\Theta_n^{\dot{x}}$. In Fig. 8 we have plotted $\ln(n_{i,n}^{T}\sqrt{T}_{i,n})$ versus $T_{i,j}$ for the particle kinetic energy coarse-grained distributions calculated from the equilibrium regime in the time ensemble. A best-fit straight line through the crosses (with $n_{i,n}^{T}\geq 20$) gave, for each particle, the temperatures shown in Table II. Again we note that, based on a Maxwellian distribution, $\dot{x}_n^2$ is an implicit function of the temperature and the system energy, Appendix B. In Fig. 9 we have used (B4) to draw the curve $\dot{x}_n^2$ versus Θ for $E_0=10$; on this graph are added the points $(\Theta_n^{\dot{x}},\overline{\dot{x}_n^2})$, where $\Theta_n^{\dot{x}}$ are the particle-velocity temperatures determined from the slopes in Fig. 8, and $\overline{\dot{x}_n^2}$ are the time-ensemble averages (see Table II). Figures 8 and 9 are evidence that the particle velocity distribution is Maxwellian.

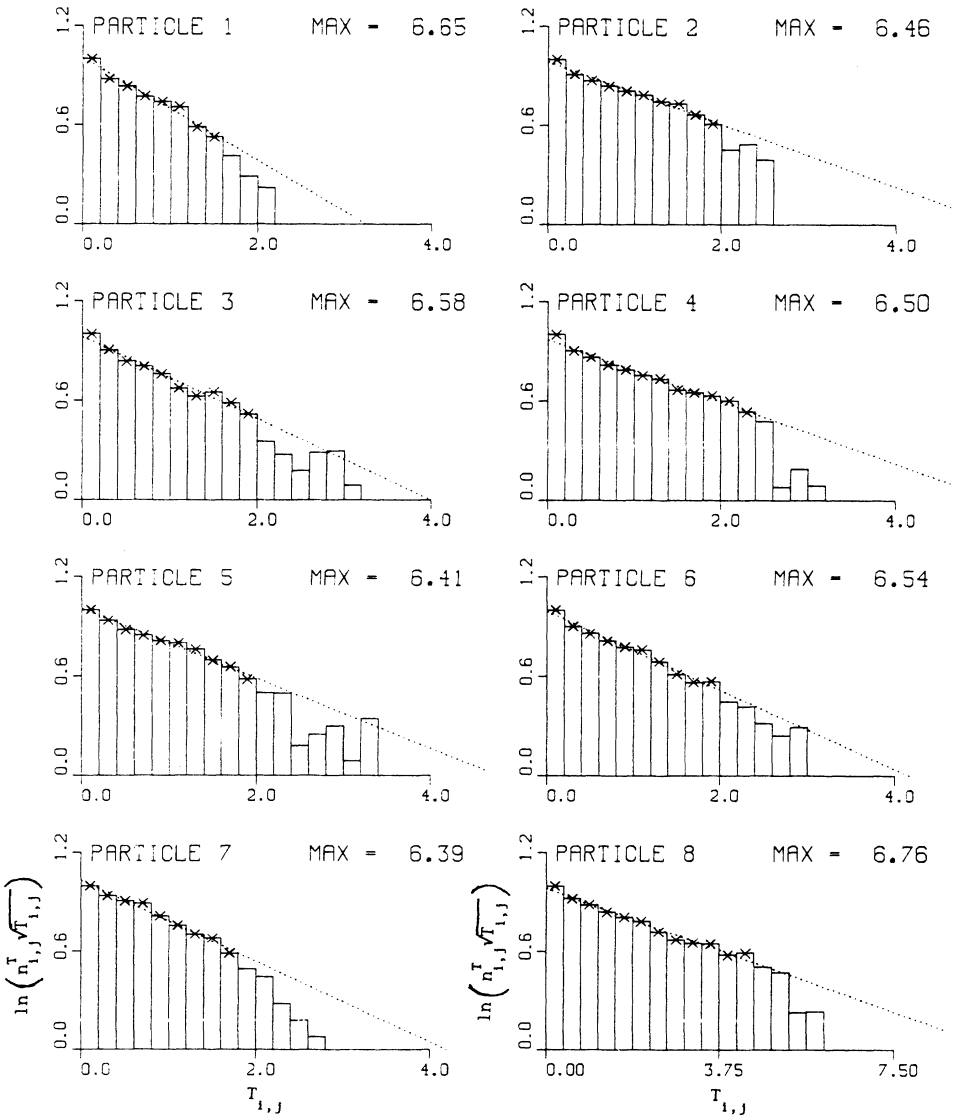

FIG. 8. Histograms of $\ln(n_{i,n}^{T}\sqrt{T}_{i,n})$ vs the partition kinetic energy $T_{i,n}$, for the first eight particles. $n_{i,n}^{T}$ is the coarse-grained kinetic energy distribution for the nth particle. The columns are normalized to the value shown in the top right corner of each graph. The crosses indicate points with $n_{i,n}\geq 20$. The dashed line is a best-fit straight line through the crosses.

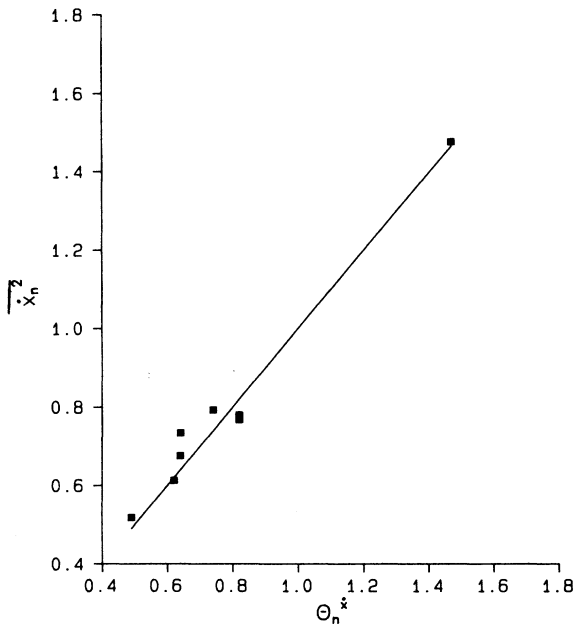

FIG. 9. Graph of the average particle velocity squared vs particle-velocity temperature, Eqs. (B4) and (B5), with system energy $E_0=10$. The squares indicate the points $(\Theta_n^{\dot{x}},\overline{\dot{x}_n^2})$, $\Theta_n^{\dot{x}}$ is the particle-velocity temperature, Table I, and $\overline{\dot{x}_j^2}$ the time average of the square of the particle velocity, Table I.

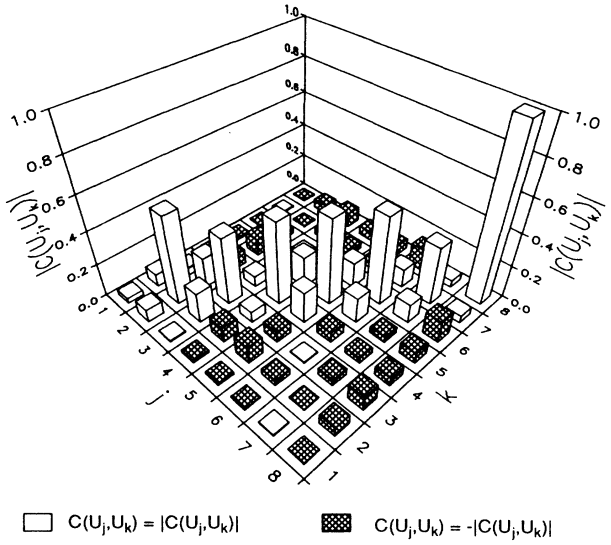

FIG. 10. Three-dimensional histogram of the correlation function $C(U_n,U_m)$ of the spring potential energies of the first eight springs. The cross hatching indicates negative values. The columns have been normalized to the maximum value $C(U_8,U_8)=0.003\,33E_0^2$.

VI. SPRING EXTENSIONS

We shall refer to the spring between the n and $n-1$ particles as the nth spring. The potential energy stored in this spring is

$$U_n \equiv \tfrac{1}{2}\xi_n^2 + \frac{\mu}{4}\xi_n^4 , \tag{25}$$

where $\xi_n \equiv x_n - x_{n-1}$ is the spring extension. The average spring energies $\overline{U}_n$, $n=1,2,\ldots,8$, were calculated from the equilibrium data in the time ensemble—these are given in Table III.

The time-ensemble correlation function $C(U_n,U_m)$ is shown in Fig. 10. The data are normalized to the largest value $C(U_8,U_8)=0.003\,33E_0^2$. The smallest diagonal element is $C(U_1,U_1)=0.000\,01E_0^2$. The off-diagonal elements range in value from

$$C(U_6,U_8)=-0.000\,44E_0^2 \text{ to } C(U_4,U_5)=0.000\,63E_0^2 . \tag{26}$$

$C(U_n,U_m)$ shows a qualitatively similar behavior to $C(\dot{x}_n^2,\dot{x}_m^2)$, see Fig. 7.

TABLE III. Time-averaged spring energies, $n=1,2,\ldots,8$. Distribution temperature for the spring extensions from equilibrium time-ensemble data.

n	$\overline{U}_n$	Θ_n^{ξ}
1	0.08	0.17
2	0.30	0.80
3	0.26	0.54
4	0.27	0.69
5	0.31	0.76
6	0.30	0.77
7	0.24	0.57
8	0.44	0.17

We assume that the distribution of the spring extension ξ_n is

$$dn_n^{\xi}=c_n\exp[-(U_n/\Theta_n^{\xi})]d\xi_n , \tag{27}$$

where c_n is a normalization constant, U_n the spring potential energy (25), and Θ_n^{ξ} the spring temperature. Hence the number of copies for which the nth spring has energy in the range $[U_n, U_n+dU_n]$ is

$$dn_n^{U}=c_n[\exp-(U_n/\Theta_n^{\xi})/(\xi_n+\mu\xi_n^3)]dU_n , \tag{28}$$

where

$$\xi_n^2=[-1+\sqrt{(1+4\mu U_n)}]/\mu . \tag{29}$$

To check the correctness of the assumption in (27), we followed the same procedure as before. The coarse-grained distribution from (28) is

$$n_{i,n}^{U}=A_n\{\exp[-(U_{i,n}/\Theta_n^{\xi})]/(\xi_{i,n}+\mu\xi_{i,n}^3)\} , \tag{30}$$

with $\xi_{i,n}$ given by (29) and spring energy set equal to the partition value, namely,

$$U_{i,n}=(i-1/2)E_0/N_n , \tag{31}$$

where $N_1=200$ and $N_n=50$, for $n=2,3,\ldots,8$. From (30) and (31), we see that $\ln[n_{i,n}^{U}(\xi_{i,n}+\mu\xi_{i,n}^3)]$ versus i is a straight line with slope proportional to the inverse of the

spring temperature Θ_n^{ξ}. We calculated the coarse-grained distributions $n_{i,n}^{U}$ from the equilibrium data in the time ensemble. In Fig. 11 we have plotted the resulting $\ln[n_{i,n}^{U}(\xi_{i,n}+\mu\xi_{i,n}^3)]$ values against the integers i. The spring temperatures determined from the best-fit straight lines are shown in Table III.

From Eq. (28), the average potential energy in the nth spring is

$$\bar{U}_n = c_n \int_0^{E_0} U_n \{\exp[-(U_n/\Theta_n^{\xi})]/[\xi(U_n) + \mu\xi^2(U_n)]\} dU_n \ , \tag{32}$$

where $\xi(U_n)$ is a solution to (29). Thus $\bar{U}_n$ is a function of Θ_n^{ξ} and E_0. We have drawn the curve $\bar{U}_n$ versus Θ_n^{ξ} for $E_0=10$ in Fig. 12; we have also added the points $(\Theta_n^{\xi}, \bar{U}_n)$, where Θ_n^{ξ} is the spring temperature calculated from the slopes in Fig. 11 and listed in Table III, and $\bar{U}_n$ are the time-ensemble averages of the spring potential energies. Figures 11 and 12 provide evidence that the spring extensions ξ_n have a Maxwellian distribution described by Eq. (27). The range of $\bar{U}_n$ values is also consistent (see remarks above on the $\overline{\dot{x}_n^2}$) with local environment similarities and differences—the $\bar{U}_n$ are qualitatively similar to the average of the $\overline{\dot{x}_n^2}$ of adjacent particles.

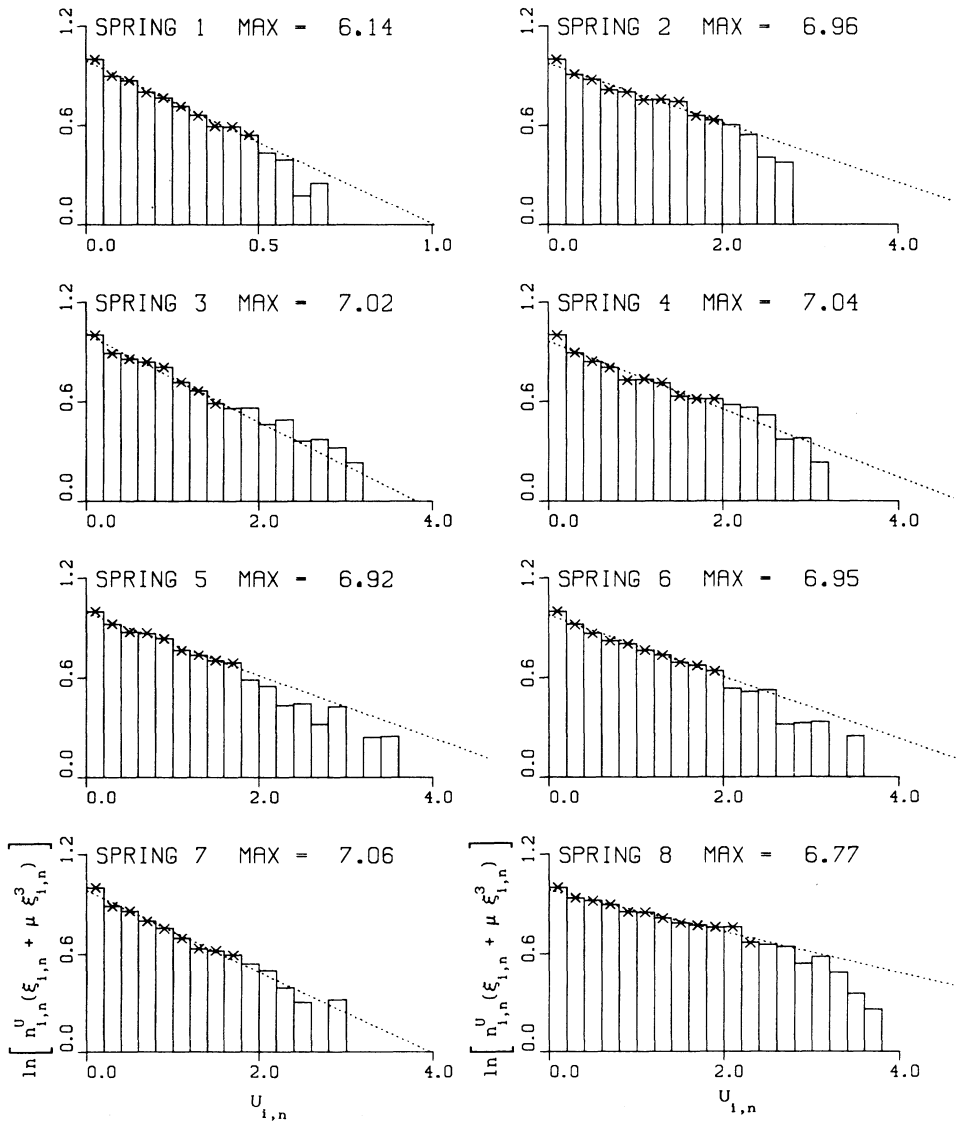

FIG. 11. Histograms of $\ln([n_{i,n}^{U}(\xi_{i,n}+\mu\xi_{i,n}^3)]$ vs the partition spring energy $U_{i,n}$ for the first eight springs. $n_{i,n}^{U}$ is the coarse-grained spring potential energy distribution for the nth spring. The columns are normalized to the value shown in the top right corner of each graph. The crosses indicate points with $n_{i,n} \geq 20$. The dashed line is a best-fit straight line through the crosses.

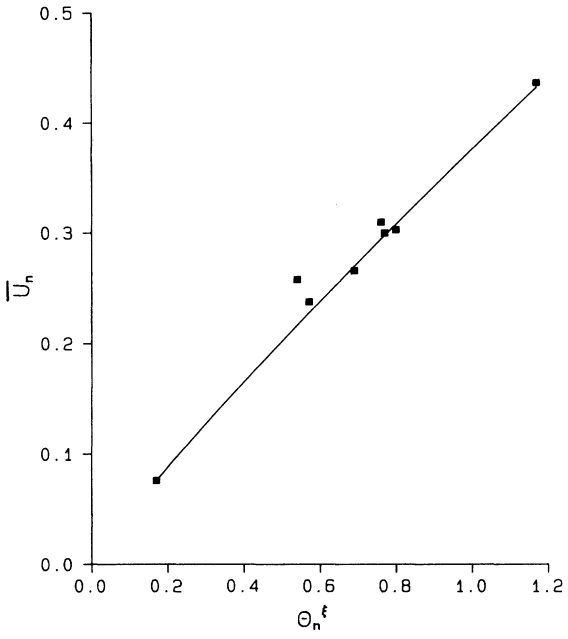

FIG. 12. Graph of the average spring potential energy vs spring-energy temperature, Eqs. (30) and (32), with system energy $E_0=10$. The squares indicate the points $(\Theta_n^\xi, \overline{U}_n)$, Θ_n^ξ is the spring temperature, Table III, and $\overline{U}_n$ the time average of the spring energy, Table III.

VII. DISCUSSION

The data described in the preceding sections indicate that in the statistical equilibrium regime of the $(15+2)$-particle chain the mode velocities $\dot{q}_j$, the particle velocities $\dot{x}_n$, and the spring extensions ξ_n each exhibit a Maxwellian distribution. Furthermore, the associated temperatures in each case are consistent with the generalized equipartition theorem (Appendix B). The agreement between the mode-velocity temperatures and the mode-energy temperatures suggests that these two quantities share the same distribution temperature. Because each mode energy contains a significant contribution from the dynamical behavior of other modes (see definition of the ε_j in Ref. 2), this result cannot be regarded as self-evident, particularly given the two-orders-of-magnitude range in the mode temperatures. As far as the particle-velocity temperatures and the spring-extension temperatures are concerned, the variation in each group is consistent with the physical arrangement. At this stage we are unable to say to what extent data-bank-size errors play a role in the variation between the temperature columns in Tables I and II.

The velocity and energy averages and correlation functions data show that (a) the mode description is the simplest, inasmuch as three modes, 11, 13, and 15, play a dominant role in determining the statistical equilibrium dynamical behavior of the chain; and (b) the behavior of these three modes is strongly correlated and quite different from the analogous harmonic case. The question of the 16-dimensional odd-mode Γ-space probability function is still open. The dominant character of the three modes, 11, 13, and 15, suggests that as a first approximation one should tackle the problem of the six-dimensional Γ-space $(q_{11},q_{13},q_{15},\dot{q}_{11},\dot{q}_{13},\dot{q}_{15})$ probability density.

ACKNOWLEDGMENTS

This work was supported by the National Sciences and Engineering Council of Canada, and the Australian Government.

APPENDIX A

We discuss the problem of calculating averages over a $(2n-1)$-dimensional sphere in a $2n$-dimensional space. Consider a $2n$-dimensional space spanned by the coordinates $(y_1,y_2,\ldots,y_{2n})$, and in this space the $(2n-1)$-dimensional sphere, radius R, determined by the quadratic form

$$y_1^2+y_2^2+\cdots+y_{2n}^2=R^2 . \tag{A1}$$

We introduce the notation

$$R_1^2\equiv R^2-y_{2n}^2-y_{2n-1}^2-\cdots-y_1^2 , \tag{A2}$$

$$R_2^2\equiv R^2-y_{2n}^2-y_{2n-1}^2-\cdots-y_2^2 , \tag{A3}$$

$$R_{2n}^2\equiv R^2-y_{2n}^2 . \tag{A4}$$

The outward normal to the sphere at the point $(y_1,y_2,\ldots,y_{2n})$ is parallel to the unit vector $(y_1/R,y_2/R,\ldots,y_{2n}/R)$. We obtain an expression for the area of this sphere by noting that the infinitesimal surface element dS projects onto the subspace $(y_2,y_3,\ldots,y_{2n})$ through the component y_1/R of the unit vector. Since the point lies on the sphere, $y_1=R_2$. Hence the surface area is

$$S_{2n}=\int_{-R}^{R}dy_{2n}\int_{-R_{2n}}^{R_{2n}}dy_{2n-1}\cdots\int_{-R_3}^{R_3}2R\,dy_2/R_2 . \tag{A5}$$

This is a $(2n-1)$-fold integral. The first integration on the right is trivial and yields the value $2\pi R$. We now choose to carry out the remaining integrations in pairs to get, after $s-1$ integrations,

$$S_{2n}=\int_{-R}^{R}dy_{2n}\int_{-R_{2n}}^{R_{2n}}dy_{2n-1}\cdots\int_{-R_{2s}}^{R_{2s}}dy_{2s-1}I_{2s-2} , \tag{A6}$$

where

$$I_{2s}\equiv\frac{2\pi^2}{(s-1)!}R_{2s+1}^{2s-2}R . \tag{A7}$$

After $2n-3$ integrations we find

$$S_{2n}=\int_{-R}^{R}dy_{2n}\int_{-R_{2n}}^{R_{2n}}dy_{2n-1}I_{2n-2} . \tag{A8}$$

Hence area of the sphere (A1) is

$$S_{2n}=\frac{2\pi^n}{(n-1)!}R^{2n-1}\ , \tag{A9}$$

in agreement with the results of Pathria.[12] We write the right-hand side of (A8) in two other different forms. First, change the variables from y_{2n},y_{2n-1} to $e=y_{2n}^2+y_{2n-1}^2$ and $\theta=\arctan(y_{2n}/y_{2n-1})$, then integrate over θ to get

$$S_{2n}=\frac{2\pi^n R}{(n-2)!}\int_0^{R^2}(R^2-e)^{n-2}de\ . \tag{A10}$$

Second, integrate over the y_{2n-1} coordinate, then

$$S_{2n}=\frac{2^{2n-2}\pi^{n-1}}{(2n-3)!}(n-2)!R \times\int_{-R}^{R}(R^2-y_{2n-1}^2)^{(2n-3)/2}dy_{2n}\ . \tag{A11}$$

If we divide both sides of Eq. (A5) by the value of the area S_{2n} in Eq. (A9), we can regard the resulting equation as a normalization condition for the probability distribution for "states" on the sphere; the probability distribution is clearly a constant equal to $1/S_{2n}$ or $(n-1)!/[2\pi^{n-1}R^{2n-1}]$. In a similar fashion we deduce from (A8), (A10), and (A11), respectively, the probability distribution for the pair of coordinates y_{2n},y_{2n-1}, namely,

$$[(n-1/\pi]R^{2-2n}(R^2-y_{2n}^2-y_{2n-1}^2)^{n-2}\ , \tag{A12}$$

the distribution for the sum of squares e,

$$[(n-1)R^{2-2n}](R^2-e)^{n-2}\ . \tag{A13}$$

and the probability distribution for the coordinate y_{2n},

$$\frac{(2^{2-2n}/\pi)(n-1)!(n-2)!}{(2n-3)!}R^{2-2n}(R^2-y_{2n}^2)^{(2n-3)/2}\ . \tag{A14}$$

It is clear from these expressions, (A12)–(A14), that the probability distribution for some set of coordinates is not a simple product of the corresponding single distributions (A14). This is a direct result of the demand that points lie on the sphere (A1).

Since the labeling of the coordinates is arbitrary, these expressions hold for any pair of labels s,t. As an example, consider the average of a function of y_{2n} and y_{2n-1} over the spherical hypersurface; from (A12), this is of the form

$$\langle f(y_{2n},y_{2n-1})\rangle=\int_{-R}^{R}dy_{2n}\int_{-R_{2n}}^{R_{2n}}f(y_{2n},y_{2n-1})[(n-1)/\pi]R^{2-2n}(R^2-y_{2n}^2-y_{2n-1}^2)^{n-2}dy_{2n-1}\ . \tag{A15}$$

As remarked above, the averages $\langle f(y_s,x_s)\rangle$ and $\langle f(y_s,y_t)\rangle$, $s\neq t$, are independent of the choice of s and t.

We find the following particular results ($s\neq t$ understood):

$$\langle y_s\rangle=0\ , \tag{A16}$$

$$\langle y_s^2\rangle=R^2/2n\ , \tag{A17}$$

$$\langle y_s y_t\rangle=0\ , \tag{A18}$$

$$\langle y_s^4\rangle=R^4/[4n(n+1)]\ , \tag{A19}$$

$$\langle y_s^2 y_t^2\rangle=R^4/[12n(n+1)]\ . \tag{A20}$$

Consider now the microcanonical ensemble for a set of eight uncoupled harmonic oscillators. We write the Hamiltonian in the form

$$H=\tfrac{1}{2}\sum_{s=1}^{8}(\dot{x}_s^2+\omega_s^2x_s^2)\ . \tag{A21}$$

The microcanonical ensemble consists of a uniform distribution of states on the spherical shell $H=E_0$ in the 16-dimensional Γ space for this system. Thus microcanonical averages are taken over the spherical shell of radius $R=\sqrt{2}E_0$. Applying the results presented above, we deduce that

$$\langle\dot{x}_s\rangle=\langle\omega_s x_s\rangle=0\ , \tag{A22}$$

$$\langle\dot{x}_s^2\rangle=\langle\omega_s^2x_s^2\rangle=E_0/8\ , \tag{A23}$$

$$\langle\dot{x}_s\dot{x}_t\rangle=\langle\dot{x}_s\omega_s x_s\rangle=\langle\dot{x}_s\omega_t x_t\rangle=\langle\omega_s x_s\omega_t x_t\rangle=0\ , \tag{A24}$$

$$\langle\varepsilon_s\rangle=E_0/8\ , \tag{A25}$$

$$\langle\dot{x}_s^4\rangle=\langle(\omega_s x_s)^4\rangle=E_0^2/24\ , \tag{A26}$$

$$\langle\dot{x}_s^2\dot{x}_t^2\rangle=\langle\dot{x}_s^2\omega_t^2x_t^2\rangle=\langle\dot{x}_s^2\omega_s^2x_s^2\rangle=\langle\omega_s^2x_s^2\omega_t^2x_t^2\rangle =E_0^2/72\ , \tag{A27}$$

$$\langle\varepsilon_s^2\rangle=E_0^2/36\ , \tag{A28}$$

$$\langle\varepsilon_s\varepsilon_t\rangle=E_0^2/72\ , \tag{A29}$$

where ε_s is the energy of the sth oscillator.

We define the correlation function of the two quantities x_s and x_t as $C(x_s,x_t)\equiv\langle x_s x_t\rangle-\langle x_s\rangle\langle x_t\rangle$. Then,

$$C(\dot{x}_s,\dot{x}_s)=C(\omega_s x_s,\omega_s x_s)=E_0/8\ , \tag{A30}$$

$$C(\dot{x}_s,\dot{x}_t)=C(\dot{x}_s,\omega_t x_t)=C(\omega_s x_s,\omega_t x_t)=0\ , \tag{A31}$$

$$C(\dot{x}_s^2,\dot{x}_s^2)=C(\omega_s^2x_s^2,\omega_s^2x_s^2)=5E_0^2/192\ , \tag{A32}$$

$$C(\dot{x}_s^2,\dot{x}_t^2)=C(\dot{x}_2^2,\omega_t^2x_t^2)=C(\omega_s^2x_s^2,\omega_t^2x_t^2)=-E_0^2/576\ , \tag{A33}$$

$$C(\varepsilon_s,\varepsilon_s)=7E_0^2/576\ , \tag{A34}$$

$$C(\varepsilon_s,\varepsilon_t)=-E_0^2/576\ . \tag{A35}$$

APPENDIX B

In this Appendix we derive an expression for the mean-square velocity in a system with an upper-energy bound. Consider a system described by a velocity v

which satisfies a Maxwellian distribution in the interval $(0,v_0)$. Thus the probability that the velocity has a value in the range $[v,v+dv]$ is

$$dn = c \exp[-(\beta v^2/2)]dv \ , \tag{B1}$$

where c is a constant and β the inverse temperature $1/\Theta$. The normalization condition is

$$1 = c \int_0^{v_0} \exp -(\beta v^2/2)dv \ , \tag{B2}$$

and the average of v^2 is

$$\langle v^2 \rangle = c \int_0^{v_0} v^2 \exp[-(\beta v^2/2)]dv \ . \tag{B3}$$

Using (B2) to eliminate the constant c, we can write $\langle v^2 \rangle$ in the form

$$\langle v^2 \rangle = \frac{1}{\beta} - 2\frac{\partial(\ln I)}{\partial \beta} = \Theta - 2\frac{\partial(\ln I)}{\partial \beta} \ , \tag{B4}$$

where

$$I \equiv \frac{\sqrt{\pi}}{2} - \int_{t_0}^{\infty} \exp(-t^2)dt \ , \tag{B5}$$

and $t_0 = (v_0^2\beta/2)^{1/2}$. Thus the mean-squared velocity $\langle v^2 \rangle$ differs from the temperature Θ by an amount determined by I. As $v_0 \to \infty$, $I \to$ a constant and hence $\langle v^2 \rangle \to \Theta$, the open system result, referred to as the equipartition principle.[4] Thus we may think of Eq. (B4) as a generalization of the equipartition principle.

[1]B. I. Henry and J. Grindlay, Phys. Lett. A **119**, 215 (1986).

[2]B. I. Henry and J. Grindlay, Physica, **28D**, 49 (1987).

[3]B. I. Henry and J. Grindlay, Phys. Rev. A **38**, 2594 (1988).

[4]R. C. Tolman, *The Principles of Statistical Mechanics* (Oxford University Press, Oxford, 1938).

[5]N. Ooyama, H. Hirooka, and N. Saito, J. Phys. Soc. Jpn. **27**, 815 (1969).

[6]D. ter Haar, *Elements of Statistical Mechanics* (Rinehart, New York, 1954).

[7]W. Pauli, in *Pauli Lectures on Physics: Volume 4, Statistical Mechanics*, edited by C. P. Enz (MIT, Cambridge, MA, 1973).

[8]We use the word "ergodic" in the usual sense, in statistical mechanics, of equivalence of averages over time and averages over copies. D. ter Haar, Rev. Mod. Phys. **27**, 289 (1955).

[9]J. Ford, in *Chaotic Dynamics and Fractals*, edited by M. F. Barnsley and S. C. Demko (Academic, New York, 1986), p. 1.

[10]D. Beeman, J. Comput. Phys. **20**, 130 (1976).

[11]A. R. Janzen and J. W. Leech, Comput. Phys. Commun. **32**, 349 (1984).

[12]R. K. Pathria, *Statistical Mechanics* (Pergammon, Oxford, 1972), Appendix C.